



Quantinuum System  
Model H1 Product Data Sheet

Version 5.10 October 3, 2022

## ■ TABLE OF CONTENTS

<b>INTRODUCTION .....</b>	<b>3</b>
<b>FEATURES .....</b>	<b>3</b>
<b>SPECIFICATIONS.....</b>	<b>3</b>
<b>SYSTEM OPERATION.....</b>	<b>4</b>
Generational Hardware Nomenclature .....	4
API Interface .....	4
Native Gate Set.....	4
Constructed gate examples using QASM notation .....	5
Mid-circuit measurement and conditional operations.....	6
Inter-circuit performance validation.....	6
Dynamic calibrations .....	6
Depth-1 circuit time .....	7
Estimating circuit time .....	7
Arbitrary Angle ZZ Gates.....	8
Single-qubit gate fidelity .....	8
Two-qubit gate fidelity .....	9
State preparation and measurement (SPAM) error .....	9
Mid-circuit measurement cross-talk error .....	9
Memory error per qubit at depth-1 circuit time .....	9
Benchmarking Data.....	10
<b>REFERENCES .....</b>	<b>10</b>

## ■ INTRODUCTION

This Product Data Sheet covers all features and characteristics of the **Quantinum System Model H1, Powered by Honeywell**. This includes specifications for all quantum computers available online, which includes quantum computers H1-1 and H1-2.

## ■ FEATURES

N ≥ 12 qubit trapped-ion based quantum computers  
All-to-all connectivity  
Laser based quantum gates  
Quantum charge-coupled device (QCCD) architecture with three or more parallel gate zones  
Mid-circuit measurement conditioned circuit branching  
Qubit reuse after mid-circuit measurement  
Native gate set: single-qubit rotations, two-qubit ZZ gates, arbitrary-angle ZZ gates

## ■ SPECIFICATIONS

Table 1 lists the specifications for Quantinum H1-1 and H1-2 quantum computers.

*Table 1 Quantinum H-Series Specifications*

System Fundamentals	H1-1			H1-2		
Parameters	min	typ	max	min	typ	max
<b>General</b>						
Qubits	20			12		
Connectivity	All-to-all			All-to-all		
Parallel two-qubit operations	5			3		
<b>Errors</b>						
Single-qubit gate infidelity	$1 \times 10^{-5}$	$4 \times 10^{-5}$	$3 \times 10^{-4}$	$2 \times 10^{-5}$	$4 \times 10^{-5}$	$3 \times 10^{-4}$
Two-qubit gate infidelity	$2 \times 10^{-3}$	$3 \times 10^{-3}$	$5 \times 10^{-3}$	$2 \times 10^{-3}$	$3 \times 10^{-3}$	$5 \times 10^{-3}$
State preparation and measurement (SPAM) error	$2 \times 10^{-3}$	$3 \times 10^{-3}$	$5 \times 10^{-3}$	$2 \times 10^{-3}$	$3 \times 10^{-3}$	$6 \times 10^{-3}$
Memory error per qubit at average depth-1 circuit	$1 \times 10^{-4}$	$4 \times 10^{-4}$	$1 \times 10^{-3}$	$1 \times 10^{-4}$	$4 \times 10^{-4}$	$1 \times 10^{-3}$
Mid-circuit measurement cross-talk error	$5 \times 10^{-6}$	$2 \times 10^{-5}$	$2 \times 10^{-4}$	$1 \times 10^{-5}$	$5 \times 10^{-5}$	$2 \times 10^{-4}$

## ■ SYSTEM OPERATION

The **Quantinuum System Model H1, Powered by Honeywell**, operates on qubits implemented through atomic hyperfine states of  $^{171}\text{Yb}^+$ . The H1 systems include two machines, the H1-1 and the H1-2, which each have twelve or more physical qubits (ions) that move, individually or in pairs, between three or more interaction zones where all quantum operations (initialization, measurement, single-, and two-qubit gates) are performed using lasers. By rearranging the physical location of the qubits, a two-qubit gate can be performed on any arbitrary pair, giving the system all-to-all connectivity. Additionally, because there are multiple interaction zones, multiple quantum operations may be performed in parallel.

Although the qubits are all identical, there may be differences in the errors associated with quantum operations depending on the location, i.e., interaction zone, in which the quantum operations take place, independent of the specific qubits that are in that location. However, the location for each quantum operation is determined by the compiler and may vary even for similar circuits, as each circuit is optimized to minimize the number of transport operations and the time required to run the circuit. The typical infidelities reported on this product data sheet are an average over all operational zones, with the minimum and maximum spanning both the difference between zones and the day-to-day variation.

### Generational Hardware Nomenclature

System Model H1 refers to a generation of quantum computing hardware using ion traps with a single linear geometry. Individual machines that use this generation of ion traps will be designated by the H1-X nomenclature, for example H1-1 and H1-2 are two separate quantum computing machines using the same ion trap design. Though the machines are based on the same architecture, it is inevitable that at any time individual machines may have different capabilities and slight differences in noise and error sources. At no time should either machine exceed the maximum allowed error specified above.

### API Interface

Communication with Quantinuum System Model H1 occurs through an API endpoint based on the OpenQASM 2.0 standard [1]. Interface details are given in the *Quantinuum Application Programming Interface (API) Specification*.

### Native Gate Set

The Quantinuum System Model H1 utilizes the following native gate set.

Native single-qubit gates:

$$U_{1q}(\theta, \varphi) = e^{-i(\cos \varphi \hat{X} + \sin \varphi \hat{Y})\theta/2} = \begin{pmatrix} \cos \frac{\theta}{2} & -ie^{-i\varphi} \sin \frac{\theta}{2} \\ -ie^{i\varphi} \sin \frac{\theta}{2} & \cos \frac{\theta}{2} \end{pmatrix}$$
$$R_z(\lambda) = e^{-i\hat{Z}\lambda/2} = \begin{pmatrix} e^{-i\lambda/2} & 0 \\ 0 & e^{i\lambda/2} \end{pmatrix}$$

Fully entangling two-qubit gate:  $ZZ() = e^{-i\frac{\pi}{4}\hat{Z}\otimes\hat{Z}} = e^{-\frac{i\pi}{4}} \begin{pmatrix} 1 & 0 & 0 & 0 \\ 0 & i & 0 & 0 \\ 0 & 0 & i & 0 \\ 0 & 0 & 0 & 1 \end{pmatrix}$

Arbitrary angle two-qubit gate:  $RZZ(\theta) = e^{-i\frac{\theta}{2}\hat{Z}\otimes\hat{Z}} = e^{-\frac{i\theta}{2}} \begin{pmatrix} 1 & 0 & 0 & 0 \\ 0 & e^{i\theta} & 0 & 0 \\ 0 & 0 & e^{i\theta} & 0 \\ 0 & 0 & 0 & 1 \end{pmatrix}$

$$RZZ\left(\frac{\pi}{2}\right) = ZZ()$$

$\hat{X}$ ,  $\hat{Y}$ , and  $\hat{Z}$  are the standard Pauli operators and the two-qubit matrix is written in the  $|0,0\rangle, |0,1\rangle, |1,0\rangle, |1,1\rangle$  basis. Currently only  $U_{1q}\left(\theta = \left\{\frac{\pi}{2}, \pi\right\}, \varphi\right)$  gates are run on the hardware, arbitrary values of  $\theta$  are executed with two single-qubit gates.

$$U_{1q}(\theta, \varphi) = U_{1q}\left(\frac{\pi}{2}, \varphi + \frac{\pi}{2}\right) R_z(\theta) U_{1q}\left(\frac{\pi}{2}, \varphi - \frac{\pi}{2}\right).$$

It is important to note that the arbitrary rotation around the z axis,  $R_z(\lambda)$ , is performed virtually within the software. All other gates are constructed from this set.

*Please note that our native  $U_{1q}(\theta, \varphi)$  gate is **NOT** IBM's standard  $U(\theta, \varphi, \lambda)$  as defined in [1].*

$$U_{1q}(\theta, \varphi) = U\left(\theta, \varphi - \frac{\pi}{2}, \frac{\pi}{2} - \varphi\right)$$

## Constructed gate examples using QASM notation

Examples using the native gate set within QASM are below.

Pauli gate: bit-flip  $x() \ a = U_{1q}(\text{pi}, 0) \ a;$

Pauli gate: bit and phase flip  $y() \ a = U_{1q}(\text{pi}, \text{pi}/2) \ a;$

Pauli gate: phase flip  $z() \ a = R_z(\text{pi}) \ a;$

Clifford gate: Hadamard  $h() \ a = U_{1q}(\text{pi}/2, -\text{pi}/2) \ a;$   
 $R_z(\text{pi}) \ a;$

Clifford gate: CNOT  $CX() \ c, t = U_{1q}(-\text{pi}/2, \text{pi}/2) \ t;$

		<code>ZZ() c, t;</code>
		<code>Rz(-pi/2) c;</code>
		<code>U1q(pi/2, pi) t;</code>
		<code>Rz(-pi/2) t;</code>
Pauli interaction: Z basis	<code>rzz(pi/4) c, t =</code>	<code>RZZ(pi/4) c, t;</code>
Pauli interaction: X basis	<code>rxz(pi/4) c, t =</code>	<code>U1q(pi/2, pi/2) c;</code>
		<code>U1q(pi/2, pi/2) t;</code>
		<code>RZZ(pi/4) c, t;</code>
		<code>U1q(pi/2, -pi/2) c;</code>
		<code>U1q(pi/2, -pi/2) t;</code>

## Mid-circuit measurement and conditional operations

Due to the internal level structure of trapped-ion qubits, a mid-circuit measurement may leave the qubit in a non-computational state. **All mid-circuit measurements should be followed by initialization if the qubit is to be used again in that circuit.** The qubit may be prepared in the measured state by calling for a measurement followed by initialization and a measurement dependent spin-flip.

When a subset of qubits is measured in the middle of the circuit, the classical information from these measurements can be used to condition future elements of the circuit. Although the laser pulses that implement both single- and two-qubit gates are conditional, the transport operations used to rearrange the physical location of the qubits are not. The qubits will be reconfigured to allow for all gates in all branches irrespective of the mid-circuit measurement outcome. In the context of memory error and run time, the effective depth of a circuit with measurement conditioned branching includes all branches.

## Inter-circuit performance validation

Jobs submitted with large shot-counts are automatically divided into appropriately sized chunks of smaller shot-counts. Chunking ensures that system state-checks and dynamic calibrations happen at the appropriate frequency. The number of shots in a chunk is dynamically chosen by the compiler and will vary with the complexity of the circuit. A series of system checks are performed before and after each chunk. If an error is detected, any suspect results are rejected and the failed chunk shots are rerun. For jobs consisting of multiple chunks, the time between the start date and result date will include all of the system checks and calibrations that happened in the middle of that job.

## Dynamic calibrations

The system automatically schedules and executes calibration routines. There are two types of automated calibrations: those that are executed on a predetermined time interval and those that are triggered when a drift tolerance is exceeded. Because the latter does not follow a predetermined schedule, the circuit throughput will vary due to these calibrations.

## Depth-1 circuit time

We define the depth-1 circuit time as the time it takes to arbitrarily permute all qubits and perform single-qubit and two-qubit gates on all  $\lfloor \frac{N}{2} \rfloor$  pairs, as shown in Figure 1, where  $P$  represents the random permutation of all qubits. Many circuits cannot be fully parallelized into a maximally dense circuit where each qubit participates in a two-qubit gate at each step of the circuit, and may have shorter depth-1 circuit times as a result.

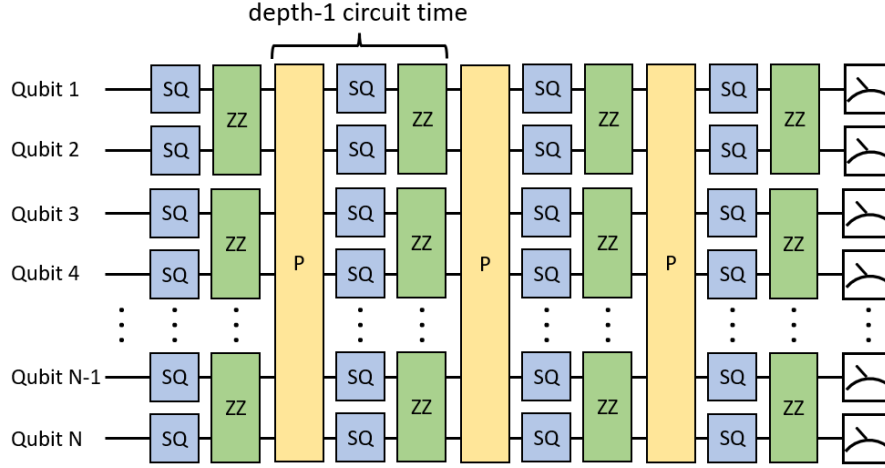


Figure 1 Depth-1 circuit time for a maximally dense circuit

## Estimating circuit time

Although the run time for a given circuit depends on many factors (both factors in the submitted circuit and the dynamic calibrations), it can be reasonably predicted using the same formula that defines H-System Quantum Credits (HQC). Typically, between 500 and 1200 HQCs can be executed in an hour. A HQC is defined as:

$$HQC = 5 + \frac{N_{1q} + 10 N_{2q} + 5 N_m}{5000} C$$

where  $N_{1q}$  is the number of single-qubit gates,  $N_{2q}$  is the number of native two-qubit gates,  $N_m$  is the number of state preparation and measurement operations in a circuit, including the initial implicit state preparation and any intermediate and final measurements and state resets, and  $C$  is the shot count. When a circuit is submitted (either to the syntax checker or H1) the cost in HQCs is returned with the results.

## Arbitrary Angle ZZ Gates

Although an arbitrary angle two-qubit entangling gate can be constructed using two fixed angle two-qubit entangling gates, a direct implementation will lower the error rate in the circuit. Not only is the number of entangling gates reduced, but the error of an  $RZZ(\theta)$  gate also scales with the angle  $\theta$ . The error on  $RZZ(\pi/2)$  is equal to the error of  $ZZ()$ .

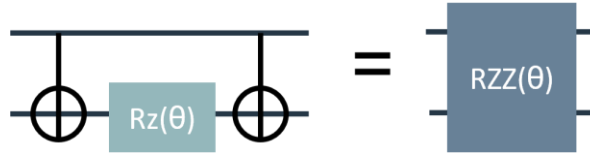


*Figure 2 Quantum circuits that use the gate sequence CNOT, RZ, CNOT can be replaced with the arbitrary angle ZZ gate. This enables a lower number of two-qubit gates in a quantum circuit, improving performance by decreasing gate errors.*

## Single-qubit gate fidelity

The single-qubit gate fidelity is measured using single-qubit randomized benchmarking (RB) with random single-qubit Clifford gates [2]. Benchmarking also uses final gate randomization, similar to Ref. [3], to fix the asymptote of the RB decay curve in order to reduce the number of fit parameters and allow fitting of shorter sequences. We run single-qubit RB with two qubits per active gate zone in parallel. The error rate is calculated by translating the RB decay curve to a per-Clifford average infidelity under the standard RB assumptions. Uncertainty is calculated from a semi-parametric bootstrap resampling of the collected data.

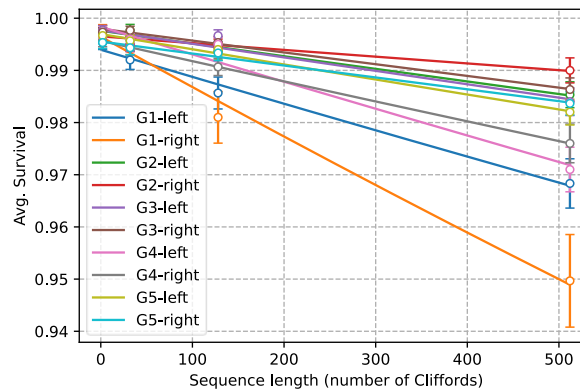


*Figure 3: Single-qubit RB data from H1-1 taken on 2022/06/09 with 2 qubits per each of the 5 gate zones. Infidelity estimates are  $5(1) \times 10^{-5}$ ,  $1.0(2) \times 10^{-5}$ ,  $2.5(7) \times 10^{-5}$ ,  $1.3(6) \times 10^{-5}$ ,  $2.6(7) \times 10^{-5}$ ,  $2.3(6) \times 10^{-5}$ ,  $5(1) \times 10^{-5}$ ,  $4(1) \times 10^{-5}$ ,  $2.9(8) \times 10^{-5}$ , and  $2.3(7) \times 10^{-5}$ .*

## Two-qubit gate fidelity

The two-qubit gate fidelity is measured with two-qubit RB using similar methods outlined above on single-qubit RB. Two-qubit RB is run with two-qubit random Clifford gates pairs of qubits in each active gate zone in parallel. The infidelity of our native entangling gate is estimated by scaling per-Clifford infidelity by the average number of entangling gates per Clifford (= 1.5).

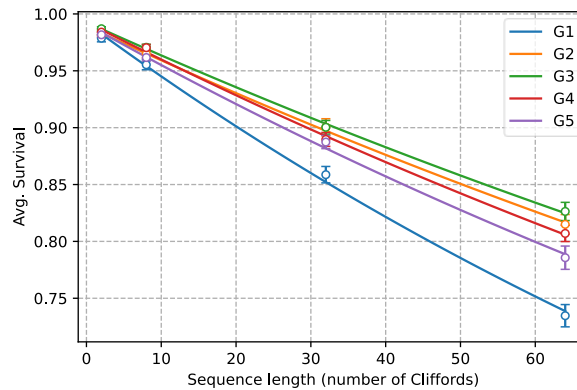


**Figure 4:** Two-qubit RB results from H1-1 taken on 2022/06/09. Gate zone 1 in blue (estimated two-qubit gate infidelity of  $3.2(3) \times 10^{-3}$ ), gate zone 2 in orange ( $2.1(3) \times 10^{-3}$ ), gate zone 3 in green ( $2.0(2) \times 10^{-3}$ ), gate zone 4 in red ( $2.3(2) \times 10^{-3}$ ), and gate zone 5 in purple ( $2.5(3) \times 10^{-3}$ ).

## State preparation and measurement (SPAM) error

The SPAM error is measured by preparing the qubits in the  $|0\rangle$  (or  $|1\rangle$ ) state and measuring to determine the fraction of time the incorrect  $|1\rangle$  (or  $|0\rangle$ ) state is returned. The reported SPAM error is the average between the  $|0\rangle$  and  $|1\rangle$  state preparation experiments. The experiment is repeated for two qubits per active gate zone and done in parallel.

## Mid-circuit measurement cross-talk error

Although qubits are physically separated during measurement, there is a small chance that an unmeasured qubit in the  $|1\rangle$  state will absorb the detection light, destroying its quantum state, and potentially scattering to the non-computational states used for state detection. This is not an issue with measurement at the end of a circuit when all qubits are measured but can impact circuits with mid-circuit measurement. The mid-circuit measurement cross-talk error is quantified by the population decay of an unmeasured qubit while applying many measurement pulses to a neighboring qubit as described in Ref. [4].

## Memory error per qubit at depth-1 circuit time

To characterize memory error in depth-1 circuit time, we perform single-qubit RB as described above, while interleaving failed conditional two-qubit gates and time delays equivalent. The failed conditional two-qubit gates are between random pairs of all available qubits and induce ion transport that would be required for dense circuits like in quantum volume. The delay time mimics the time required for sideband cooling before two-qubit gates. The net RB error measured is the average single-qubit error due to depth-1 circuits. We perform this test for all available qubits in the system.

## Benchmarking Data

The data for the measurements in this document can be found online at: <https://github.com/CQCL/quantinuum-hardware-specifications>. This repository contains the raw data along with the analysis code. For completeness a subset of the measurements are described below.

## ■ REFERENCES

- [1] A. W. Cross, L. S. Bishop, J. A. Smolin and J. M. Gambetta, "Open Quantum Assembly Language," *arXiv:1707.03429v2*, 2017.
- [2] E. Magesan, J. M. Gambetta and J. Emerson, "Characterizing quantum gates via randomized benchmarking," *Phys. Rev. A*, vol. 85, no. 4, p. 042311, 2012.
- [3] R. Harper, I. Hincks, C. Ferrie, S. T. Flammia and J. J. Wallman, "Statistical analysis of randomized benchmarking," *Phys. Rev. A*, vol. 99, no. 5, p. 052350, 2019.
- [4] J. P. Gaebler, C. H. Baldwin, S. A. Moses, J. M. Dreiling, C. Figgatt, M. Foss-Feig, D. Hayes and J. M. Pino, "Suppression of midcircuit measurement crosstalk errors with micromotion," *Phys. Rev. A*, vol. 104, no. 6, 2021.